Extended families of critical and stationary droplets for nonequilibrium phase transitions in spatially discrete bistable systems

Chi-Jen Wang ◎,[1] Da-Jiang Liu ◎,[2] and James W. Evans ◎[2,3]

[1]*Department of Mathematics, National Chung Cheng University, Chiayi 62102, Taiwan*
[2]*Ames Laboratory—USDOE, Iowa State University, Ames, Iowa 50011, USA*
[3]*Department of Mathematics and Department of Physics & Astronomy, Iowa State University, Ames, Iowa 50011, USA*

Bistable nonequilibrium systems are realized in catalytic reaction-diffusion processes, biological transport and regulation, spatial epidemics, etc. Behavior in spatially continuous formulations, described at the mean-field level by reaction-diffusion type equations (RDEs), often mimics that of classic equilibrium van der Waals type systems. When accounting for noise, similarities include a discontinuous phase transition at some value, p_{eq}, of a control parameter, p, with metastability and hysteresis around p_{eq}. For each p, there is a unique critical droplet of the more stable phase embedded in the less stable or metastable phase which is stationary (neither shrinking nor growing), and with size diverging as $p \to p_{eq}$. Spatially discrete analogs of these mean-field formulations, described by lattice differential equations (LDEs), are more appropriate for some applications, but have received less attention. It is recognized that LDEs can exhibit richer behavior than RDEs, specifically propagation failure for planar interphases separating distinct phases. We show that this feature, together with an orientation dependence of planar interface propagation also deriving from spatial discreteness, results in the occurrence of entire families of stationary droplets. The extent of these families increases approaching the transition and can be infinite if propagation failure is realized. In addition, there can exist a regime of generic two-phase coexistence where arbitrarily large droplets of either phase always shrink. Such rich behavior is qualitatively distinct from that for classic nucleation in equilibrium and spatially continuous nonequilibrium systems.

I. INTRODUCTION

Diverse nonequilibrium phenomena such as nonlinear reaction-diffusion processes in catalysis, transport, and regulation in cell biology; population dynamics in ecology; spatial epidemics, etc., often exhibit bistability of steady states for a range of some control parameter, p, as well as front propagation between coexisting states [1–5]. Behavior is typically described for spatially continuous models at the mean-field level by reaction-diffusion equations (RDEs) of the Nagumo or Cahn-Allen type [2]. In the presence of noise, these systems generally exhibit a discontinuous phase transition between steady states at some $p = p_{eq}$. Associated metastability, hysteresis, and nucleation phenomena occur for p near p_{eq}. This behavior is similar to that in classic van der Waals type descriptions of phase transitions for systems in thermodynamic equilibrium.

Away from p_{eq}, the steady states are not equally stable, the more stable one displacing the less stable one separated from it by a planar interface. The propagation velocity vanishes as $p \to p_{eq}$, a criterion consistent with and replacing the Maxwell construction for equilibrium systems [2,6]. Of particular interest is nucleation of the more stable state starting from the less stable (metastable) state wherein fluctuations induce droplets of the former embedded in the latter. Growth is inhibited by curvature at the droplet interface, but these droplets can grow indefinitely if above a critical size. An unstable stationary critical droplet exists at this unique size,

and smaller droplets shrink. As $p \to p_{eq}$, the more stable state is less effective at displacing the less stable state, and the critical size diverges [2,6]. We note that the free energy framework for thermodynamic systems, which facilitates assessment of equistability and nucleation phenomena, is lacking in nonequilibrium systems, as generally is the possibility even to construct a Lyapunov functional mimicking free energy. However, this complication may open the possibility of more diverse behavior.

Contrasting the above continuum formulations, a spatially discrete setting is arguably more appropriate for many nonequilibrium bistable phenomena. This applies for heterogeneous catalysis on crystalline surfaces at high pressure which imposes characteristic length scales of a few lattice constants [7,8]; signal propagation along myelinated nerve fibers, and other biological phenomena reflecting discrete cellular structure [9]; bistable phenomena in networks with a random or regular topology [10,11]; spread of spatial epidemics through a periodic grid of urban households [12]; and also certain electromagnetic circuits [13], atomistic-level descriptions of crystal growth [14], etc. Within a mean-field description, the above RDEs are replaced by analogous lattice differential equations (LDEs) [15]. It is well recognized that LDEs exhibit richer and more subtle behavior than RDEs, specifically propagation failure (PF) or pinning of planar interfaces [14–19]. Pinning produces stationary planar interface states which exist over a finite range of some relevant control
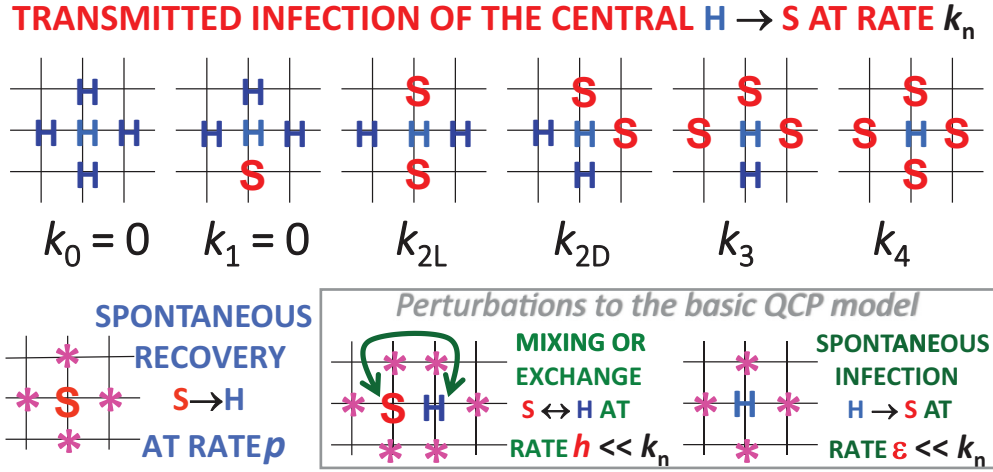
FIG. 1. Schematic of the quadratic contact process (QCP) on a square grid and perturbations thereof. H (S) denotes healthy (sick). "*" can be either H or S and does not affect the rate for the indicated process.

parameter. This type of pinning behavior has been explored in the material science, chemical and nonlinear physics, and applied mathematics communities. In addition, LDEs exhibit an orientation dependence of interface propagation and equistability not seen in isotropic continuum models. These features naturally impact assessment of equistability of states. In the context of stochastic particle models, orientation-dependent interface propagation leads to so-called generic two-phase coexistence [20–22].

The above mean-field LDE analysis of interface propagation and failure on regular lattices has specifically focused on planar interfaces. However, the topic on which we focus is droplet dynamics again on regular lattices, which involves curved interfaces. In particular, we explore phenomena related to PF. One might anticipate that the presence of PF could facilitate the formation of localized stationary droplet states which are stable. We will show that this is the case. However, since pinned fronts may only exist for selected orientations, one cannot simply regard localized stationary states as a combination of pinned fronts with different orientations. A primary motivation for consideration of droplet dynamics is that it underlies nucleation phenomena in bistable systems. In continuum models, stationary droplet states correspond to so-called critical droplets, which, however, are unstable [2,23]. It should be noted that localized stationary states have been observed previously for bistable models in spatially discrete systems, which, however, incorporated a random scale-free and hierarchical network structure, or a treelike spatial structure [10,11]. These studies present the challenge of separating the effect of the random or nonperiodic topological spatial structure on localization from the intrinsic nature of the model kinetics. In this respect, we note the generic potential for randomization to induce localization [24]. However, our analysis of such phenomena on regular periodic lattices allows natural connection to nucleation phenomena, and specifically critical droplets, addressing fundamental questions related to the effect of curvature on interface propagation.

In this study, we will perform a mean-field LDE analysis of variations of the quadratic contact process (QCP)

on a square lattice [12,22] describing spatial epidemics involving infection and spontaneous recovery of individuals or households arranged on a periodic square grid. As discussed further below, the QCP is equivalent to a lattice version of Schloegl's second model for autocatalysis [25]. Our analysis will reveal PF, generic two-phase coexistence, and an unprecedented richness in behavior for critical and stationary droplets. Entire families of stationary droplets emerge with some diverging in size in regimes of propagation failure. This behavior is qualitatively distinct and far more diverse than that found for classic nucleation in equilibrium systems and in continuum models for nonequilibrium systems.

II. MODEL DESCRIPTION AND EVOLUTION EQUATIONS

A. Model description

In the QCP considered here, households or individuals arranged at sites on a square lattice are either sick (S) or healthy (H). If S, they can spontaneously recover, S → H, at rate p. If H, they can be infected by transmission of disease in the event of two or more sick neighbors, H + 2S → 3S. The infection rate, k_n, depends on the number, $n \leqslant 4$, of sick neighbors with $k_0 = k_1 = 0$. For $n = 2$, we allow the flexibility to assign different rates for "linear" (L) and "diagonal" (D) configurations with the two sick neighbors on opposite sides of the H (k_{2L}) and on diagonally adjacent sites (k_{2D}). See Fig. 1. Possible assignments include $k_{n \geqslant 2} = 1$ (threshold choice) [26–28], $k_n = n(n-1)/12$ (combinatorial choice) [27,29], or $k_{2L} = 0$, $k_{2D} = \frac{1}{4}$, $k_3 = \frac{1}{2}$, $k_4 = 1$ (Durrett choice) [12,22]. All assignments suffer from a "quirk" that infection cannot penetrate a semi-infinite healthy region with a vertical or horizontal boundary, for any $p \geqslant 0$ (i.e., even for very slow recovery). Why? All healthy sites at the boundary of this healthy region have at most one infected neighbor. Thus, vertical (or horizontal) interfaces between healthy and infected regions can only move into the infected state. Similarly, infection cannot expand beyond an infected rectangular patch or "droplet."

It is convenient to remove this quirk by perturbing the model. One can introduce "mixing" allow neighboring H and S to exchange places with small rate h [30]. Alternatively, in addition to infection requiring at least two sick neighbors, one can also allow spontaneous infection, or instead transmitted infection from a single sick neighbor [31] (in the spirit of a conventional contact process [32]), with small rate ε. We will focus on behavior for the Durrett version of the QCP allowing mixing with $h = 0.01$.

As an aside, replacing S by X, and H by $\varnothing$, this QCP becomes equivalent to a version of Schloegl's second model for autocatalysis [2,25] involving spontaneous annihilation, $X \to \varnothing$, of particles, X, residing at the sites of a square lattice at rate p, and autocatalytic creation of particles at empty sites, $\varnothing$, induced by neighboring particle pairs, $\varnothing + 2X \to 3X$ [22]. QCP model perturbation by mixing corresponds to introducing particle hopping to neighboring empty sites at rate h, and perturbation by spontaneous infection corresponds to spontaneous particle creation at empty sites at rate ε.

B. Mean-field evolution equations

Returning to the QCP perturbed by mixing, our analysis tracks the evolution of the probability, $P_{i,j}$ that site (i, j) on the square lattice is in state S, so $1 - P_{i,j}$ gives the probability that the site is in state H. Model behavior is described by the LDE,

$$d/dt \, P_{i,j} = -pP_{i,j}(\text{recovery}) + \Re_{i,j}(1 - P_{i,j})(\text{infection})$$
$$+ \, h\Delta P_{i,j}(\text{mixing}), \qquad (1)$$

where $\Delta P_{i,j} = P_{i+1,j} + P_{i-1,j} + P_{i,j+1} + P_{i,j-1} - 4P_{i,j}$ is a discrete Laplacian. The recovery term is clearly exact even in the presence of spatial correlations, but this also applies for the mixing term [33]. A closed expression for the rate of infection, $\Re_{i,j}$, of a healthy site (i, j) is obtained at the mean-field level ignoring correlations between the state of different sites. One sums contributions from all configurations of neighbors to the healthy site with two or more S, weighting by the appropriate infection rate. For example, if sites $(i \pm 1, j)$ are S and sites $(i, j \pm 1)$ are H, the contribution is $k_{2L}P_{i+1,j}P_{i-1,j}(1 - P_{i,j+1})(1 - P_{i,j-1})$.

In the following, we just consider the Durrett choice of rates which yields

$$\Re_{i,j} = \tfrac{1}{4}(P_{i+1,j}P_{i,j+1} + P_{i+1,j}P_{i,j-1}$$
$$+ \, P_{i-1,j}P_{i,j-1} + P_{i-1,j}P_{i,j+1}), \qquad (2)$$

after some simplification using binomial summation formulas [34,35]. Behavior of the QCP for other rate choices is qualitatively similar, although $\Re_{i,j}$ differs [36]. Naturally, some simplification of (1) and (2) is achieved for planar interfaces. For example, in the case of a vertical interface where $P_{i,j} = P_i$ is independent of j, then $\Delta P_{i,j}$ reduces to $\Delta P_i = P_{i+1} + P_{i-1} - 2P_{i,j}$, and $\Re_{i,j}$ reduces to $\Re_i = \tfrac{1}{2}(P_{i+1}P_i + P_{i-1}P_i)$.

It is appropriate to note behavior for spatially homogeneous states with $P_{i,j} = P$ (the probability that any household is sick) where Eq. (1) reduces to [34,35]

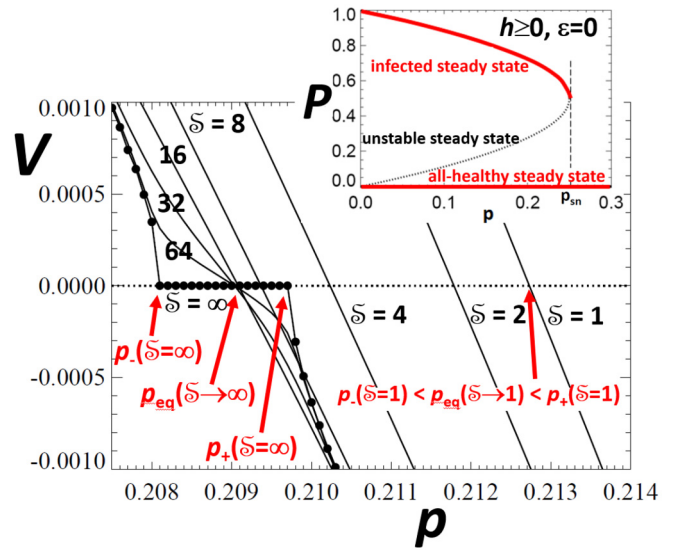$$d/dt \, P = R(P) \quad \text{where} \quad R(P) = -pP + P^2(1 - P). \qquad (3)$$

FIG. 2. Propagation velocity, V, versus p for planar interfaces separating the infected and all-healthy states for various orientations, $\mathbb{S}$, in the perturbed QCP with $h = 0.01$. For $V > 0$, infected invades all-healthy. PF occurs for $\mathbb{S} = 1$, but for a far narrower range of p than for $\mathbb{S} = \infty$ (or $\mathbb{S} = 0$). Inset: homogeneous steady states.

yielding an all-healthy steady state with $P = 0$, for all $p \geqslant 0$, and stable (+) and unstable (−) populated steady states with $P^\pm(p) = \tfrac{1}{2} \pm \tfrac{1}{2}(1 - 4p)^{1/2}$, for $0 \leqslant p \leqslant p_{sn}$ (the regime of bistability) with upper spinodal or sn-bifurcation point $p_{sn} = \tfrac{1}{4}$. Figure 2 (inset) illustrates this equation of state.

It should be noted that there have been multiple previous mean-field implementations of spatially discrete heterogeneous versions of Schloegl's second model or QCP type models [10,11,15–19]. However, relative to our model above, these typically incorporate simpler traditional spatial coupling of the form $d/dt \, P_{i,j} = R(P_{i,j}) + k\Delta P_{i,j}$. More complex spatial coupling should generally be expected in spatially discrete "contact" models where infection or reaction involves interaction between a site and its local neighborhood. For stochastic models, this coupling is captured in a set of exact spatially heterogeneous master equations [8,34,35].

Finally, we briefly comment on our numerical analysis of the model. It is necessary to truncate this infinite coupled set of equations for $P_{i,j}$. However, this is readily achieved since the region in which $P_{i,j}$ varies is localized, and behavior in asymptotic regions is uniform adopting a value corresponding to one of the two steady states. Thus, one just appropriately sets the values of $P_{i,j}$ on the boundary of a finite domain with spatial variation confined to the central portion of that domain. Numerical integration of Eq. (1) uses a forward difference algorithm. To assess stationary droplets, Eq. (1) is generally integrated up to $t \approx 5 \times 10^5$. However, integration is extended up to $t \approx 10^7$ for p near critical values where droplet sizes diverge, especially near $p_-(\mathbb{S} = \infty)$ or $p_+(\mathbb{S} = 1)$. For near-stationary behavior, a longer time step $\Delta t = 1$ can be employed in the long-time regime. As alluded to above, in the analysis of planar interface propagation with interface slope $\mathbb{S}$, some simplification of the evolution equations is possible. $P_{i,j}$ depend only on the combination $\mathbb{S}i - j$, so Eq. (1) reduces

TABLE I. Key p values for QCP with mixing at rate $h = 0.01$, and also for $h = 0$ and $h \to 0$.

	$p_-(\mathbb{S} = \infty)$	$p_{eq}(\mathbb{S} \to \infty)$	$p_+(\mathbb{S} = \infty)$	$p_-(\mathbb{S} = 1)$	$p_{eq}(\mathbb{S} \to 1)$	$p_+(\mathbb{S} = 1)$
$h = 0$ $(h \to 0)$	0 (0.196134)	0.205051	0.207107	0.211375	0.211376	0.211378
$h = 0.01$	0.208051	0.209034	0.209721	0.2127 2978	0.2127 3015	0.2127 3055

to an infinite coupled set of equations $P_m = P_{\mathbb{S}i-j}$ labeled by a single parameter, m.

III. PLANAR INTERFACE PROPAGATION

Results for the propagation velocity, V, of planar interfaces between all-healthy and infected states in the bistable regime for $0 \leqslant p \leqslant p_{sn}$ are summarized in Fig. 2 for the perturbed Durrett version of QCP with $h = 0.01$. $V > 0$ corresponds to the infected state displacing the all-healthy state, and $V < 0$ to the opposite. Interface orientation is labeled by the slope $\mathbb{S}$. This analysis is a prerequisite for our subsequent elucidation of dynamics of droplets. For $h = 0.01$, PF or pinning is found for (i) vertical interfaces ($\mathbb{S} = \infty$) for $0.208\,09 \approx p_-(\mathbb{S} = \infty) < p < p_+(\mathbb{S} = \infty) \approx 0.209\,72$ (the same applies by symmetry for horizontal interfaces), and (ii) diagonal interfaces ($\mathbb{S} = 1$) for a far narrower regime of $0.212\,729\,78 \approx p_-(\mathbb{S} = 1) < p < p_+(\mathbb{S} = 1) \approx 0.212\,730\,55$. If $\Delta p(\mathbb{S}) = p_+(\mathbb{S}) - p_-(\mathbb{S})$, then $\Delta p(\mathbb{S} = 1)/\Delta p(\mathbb{S} = \infty) \approx 0.000\,47$.

For $\mathbb{S} \neq 1$ or ∞, there is no propagation failure, and instead there exists a unique equistable $p = p_{eq}(\mathbb{S})$ with the interface velocity $V(\mathbb{S}) \sim p - p_{eq}(\mathbb{S})$ varying quasilinearly through zero at $p = p_{eq}(\mathbb{S})$ where the interface is stationary. It is natural to consider behavior for near-vertical interfaces where we find that $p_{eq}(\mathbb{S} \to \infty) \approx 0.209\,03$ is between $p_\pm(\mathbb{S} = \infty)$ for $h = 0.01$. See Fig. 2. Similarly, for near-diagonal interfaces, we find that $p_{eq}(\mathbb{S} \to 1) \approx 0.212\,730\,15$ is between $p_\pm(\mathbb{S} = 1)$ for $h = 0.01$.

As an aside, we note that $p_\pm(\mathbb{S} = 1$ or $\infty)$ and $p_{eq}(\mathbb{S} \to 1$ or $\infty)$ depend weakly on small h. Values converge as $h \to 0$ with limits close to those for $h = 0.01$. See Table I. This applies for $p_-(\mathbb{S} = \infty) \to 0.196\,13$ as $h \to 0$, even though $p_-(\mathbb{S} = \infty) = 0$ for $h = 0$ due to the above-mentioned quirk in the unperturbed QCP.

IV. OVERVIEW OF DROPLET BEHAVIOR

It is instructive to recall the basic features of the equilibrium droplet or cluster shapes in Hamiltonian systems based on the Wulff construction, and to note Frank's description of growth shapes based on its kinetic analog [37,38]. For two-dimensional (2D) equilibrium lattice-gas models, a line tension is determined for each orientation of the cluster perimeter. Then, for the equilibrium shape, the distance from the cluster center to each point on the periphery is proportional to the line tension for the orientation at that point. This prescription also applies for critical droplets. A consequence is that orientations with high line tension tend to be absent. Frank's model for growth shapes assigns an orientation-dependent growth velocity at each point on the perimeter. Then, in the kinetic Wulff prescription for growing cluster shape, line tension for equilibrated clusters is just

replaced by growth velocity. This implies that faster propagating orientations tend to "grow out" leaving a cluster shape dominated by the slowest growing orientations.

For the Durrett version of the QCP perturbed by mixing, we consider both droplets of the infected phase embedded in the all-healthy phase, and all-healthy droplets imbedded in the infected phase. We first restrict attention to droplets having the fourfold rotational symmetry of the underlying 2D square lattice. We determine the size (i.e., area) of embedded infected droplets from $A_I = \sum_{i,j} P_{i,j}/P^+(p)$, and of embedded all-healthy droplets from $A_H = \sum_{i,j} [P^+(p) - P_{i,j}]/P^+(p)$. Droplet behavior for $h = 0.01$ is summarized in Fig. 3. It is instructive to describe behavior separately in five distinct p regimes:

(1a) For slow recovery $0 < p < p_-(\mathbb{S} = \infty)$, the macroscopic infected state is unambiguously more stable than the all-healthy state, and displaces the latter separated from it by any planar interface. However, growth of infected droplets embedded in the all-healthy state is inhibited by curvature. They only grow above a critical size $A_I^{c+}(p)$ that diverges as $p \to p_-(\mathbb{S} = \infty)$. Their shapes reflect the slowest growing horizontal and vertical orientations, and are predominantly square. Infected droplets below a critical size $A_I^{c-}(p)$ shrink due to larger curvature. $A_I^{c\pm}(p)$ are coincident for lower p, but one generally finds that $A_I^{c-}(p) < A_I^{c+}(p)$ for p above about
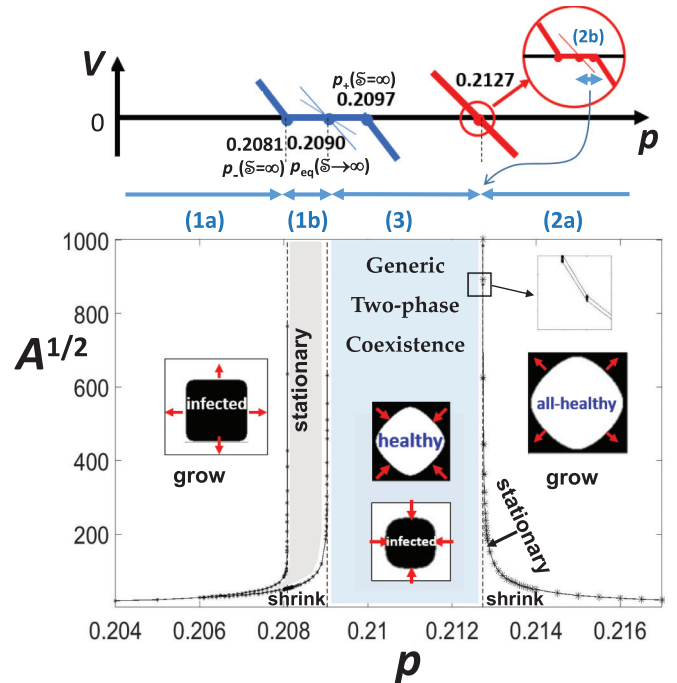

FIG. 3. Summary of the evolution and stationarity of droplets of effective linear size $A^{1/2}$ from LDE analysis of the Durrett model perturbed by mixing with rate $h = 0.01$.
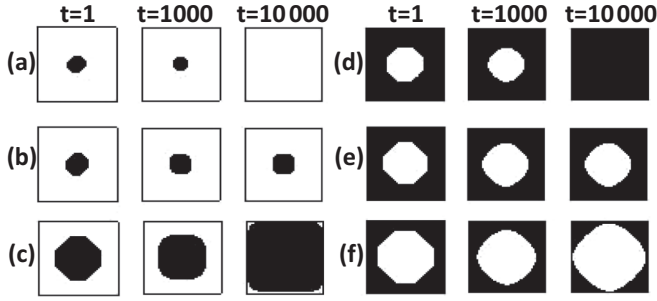
FIG. 4. Dynamics of (a–c) infected droplets embedded in the all-healthy state for $p = 0.206$, and (d–f) all-healthy droplets embedded in the infected state for $p = 0.214$. Image size: 100×100 lattice sites.

0.2060. A discrete set of stationary droplets exists within these limits, the number of which increases and diverges for increasing $p \to p_-(\mathbb{S} = \infty)$.

(1b) For $p_-(\mathbb{S} = \infty) < p < p_{\text{eq}}(\mathbb{S} \to \infty)$, again small infected droplets embedded in the all-healthy state shrink below a critical size $A_I^{c-}(p)$, which diverges as $p \to p_{\text{eq}}(\mathbb{S} \to \infty)$. All larger droplets evolve to one of an infinite discrete set of stationary infected droplets with square shape, i.e., no droplets grow indefinitely. This behavior can be readily understood as stationarity (PF) of vertical and horizontal interfaces in this regime blocks unlimited growth of infected droplets.

(2a) For rapid recovery $p_+(\mathbb{S} = 1) < p < p_{\text{sn}} = \frac{1}{4}$, the macroscopic all-healthy state is unambiguously more stable than the infected state. Analogous to (1a), all-healthy droplets embedded in the infected state only grow above a critical size $A_I^{c+}(p)$, which diverges as $p \to p_+(\mathbb{S} = 1)$. Their shapes reflect the slowest growing diagonal orientations, and are predominantly diamond shaped. All-healthy droplets shrink below a critical size $A_H^{c-}(p)$ which coincides with $A_H^{c+}(p)$ for higher p, but generally $A_H^{c-}(p) < A_H^{c+}(p)$ for p below about 0.212 77. A discrete family of stationary droplets occurs within these limits increasing and diverging in number for decreasing $p \to p_+(\mathbb{S} = 1)$.

(2b) For $p_{\text{eq}}(\mathbb{S} \to 1) < p < p_+(\mathbb{S} = 1)$, again small all-healthy droplets embedded in the infected state shrink below a critical size $A_h^{c-}(p)$ which diverges as $p \to p_{\text{eq}}(\mathbb{S} \to 1)$. Analogous to (1b), all larger droplets evolve to one of an infinite discrete family of stationary droplets with diamond shape, i.e., none grows indefinitely due to PF of diagonal

interfaces. However, given the large values of $A_h^{c-}(p)$, this behavior is difficult to assess numerically.

(3) For $p_{\text{eq}}(\mathbb{S} \to \infty) < p < p_{\text{eq}}(\mathbb{S} \to 1)$, both infected and all-healthy droplets embedded in the other state always shrink. The shapes of shrinking droplets are controlled by the fastest shrinking orientations. Thus, shrinking all-healthy droplets are effectively diamond shaped. Shrinking infected droplets are effectively square (or at least have periphery orientations close to vertical and horizontal). We identify this regime as one of generic two-phase coexistence since each state is stable against local perturbations of the other state (where such perturbations are ultimately extinguished). This feature does not apply for the other regimes.

V. DETAILED ANALYSIS OF DROPLET DYNAMICS AND STATIONARITY

Again we consider exclusively the Durrett version of the QCP perturbed by mixing with $h = 0.01$.

A. Breakdown of traditional critical droplet behavior

Behavior for "extremes" of p exhibits somewhat traditional behavior. For low $p \leqslant 0.2060$ [which is below $p_-(\mathbb{S} = \infty) \approx 0.208\,09$], and high $p \geqslant 0.212\,77$ [above $p_+(\mathbb{S} = 1) \approx 0.212\,73$], there exists a unique symmetric infected critical droplet. For $p = 0.2060$, Figure 4(a) [4(c)] shows shrinkage (growth) for infected droplets below (above) the unique critical size of $A_I^c = 735.57$. Figure 4(b) shows evolution to this stationary critical infected droplet. For $p = 0.2140$, Fig. 4(d) [4(f)] shows shrinkage (growth) for all-healthy droplets below (above) the unique critical size of $A_H^c = 2442.33$, and Fig. 4(e) shows evolution to the stationary critical all-healthy droplet. In all cases, we start with an octagonal droplet.

To illustrate the breakdown of the traditional picture of a unique unstable critical droplet, we first consider behavior for infected droplets for various $p < p_{\text{eq}}(\mathbb{S} \to \infty) \approx 0.209\,03$. Figure 5(a) shows the evolution of droplet size for a range of initial sizes at $p = 0.2060$, and indicates a finite basin of attraction (with nonzero measure) to the unique symmetric stationary droplet. Thus, this "critical" droplet constitutes a *stable* stationary solution of the LDE contrasting continuum formulations where the critical droplets constitute *unstable* stationary solutions. We attribute this stability to an enhanced propensity for stationary solutions in spatially discrete
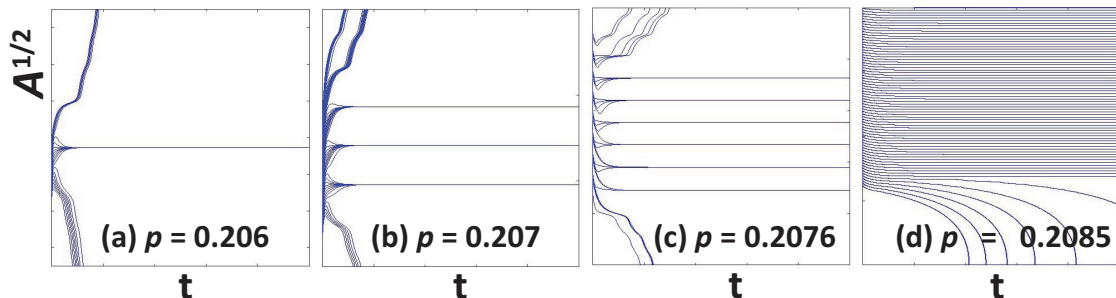

FIG. 5. Evolution of $A^{1/2}$ for infected droplets embedded in the all-healthy state for $p = 0.206$, 0.207, $0.2076 < p_-(\mathbb{S} = \infty)$, and for $p_-(\mathbb{S} = \infty) < p = 0.2085 < p_{\text{eq}}(\mathbb{S} \to \infty)$. Axes range: see Supplemental Material [39].
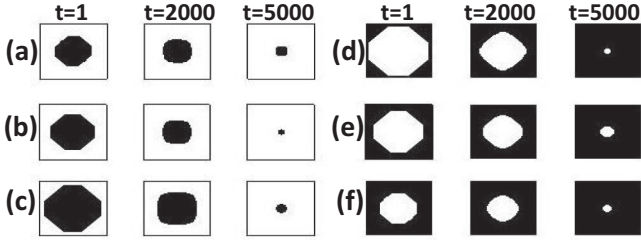
FIG. 6. Shrinking droplet dynamics for $0.209\,03 \approx p_{eq}(\mathbb{s} \to \infty) < p < p_{eq}(\mathbb{s} \to 1) \approx 0.212\,730$. Infected droplet: (a) $p = 0.2095$; (b) $p = 0.211$; (c) $p = 0.2125$. All-healthy droplet: (d) $p = 0.2095$; (e) $p = 0.211$; (f) $p = 0.2125$. Image size: 100×100 lattice sites.

systems. Figures 5(b) and 5(c) show that for evolution at $p = 0.2070$ and $p = 0.2076$ [still below $p_-(\mathbb{s} = \infty) \approx 0.208\,09$], the basin of attraction decomposes into an increasing number of sub-basins for distinct stable stationary droplets where this number and the maximum droplet size diverge as $p \to p_-(\mathbb{s} = \infty)$. A more comprehensive listing of the sizes of stationary droplets in this regime is provided in the Supplemental Material [39]. Finally, at $p = 0.2085$ [above $p_-(\mathbb{s} = \infty)$ but still below $p_{eq}(\mathbb{s} \to \infty) \approx 0.209\,03$], Fig. 5(d) reveals a semi-infinite family of stationary droplets the smallest of which has size $A_{I}^{c^-} = 4761.76$.

An analogous breakdown of the traditional picture applies for all-healthy droplets for $p > p_{eq}(\mathbb{s} \to 1) \approx 0.212\,730\,1$ upon lowering p. Figures 4(d)–4(f) show that the traditional picture still applies for $p = 0.214$, but one has two stationary droplets for $p = 0.212\,76$, three for $p = 0.212\,74$, etc. (see the Supplemental Material [39] for further details), and an infinite number for $p < p_+(\mathbb{s} = 1)$.

B. Regime of generic two-phase coexistence

For $0.209\,03 \approx p_{eq}(\mathbb{s} \to \infty) < p < p_{eq}(\mathbb{s} \to 1) \approx 0.212\,730\,2$, we have noted that both infected and all-healthy droplets embedded in the other state always shrink. Examples of this behavior are shown in Fig. 6. For infected droplets starting with an octagonal shape, diagonal portions of the periphery expand since $V(\mathbb{s} \approx 1) > 0$. This leads to a roughly square shape which starts to shrink since $V(\mathbb{s} \approx 0 \text{ or } \infty) < 0$. Similarly for all-healthy droplets starting with an octagonal shape, horizontal and vertical portions of the periphery expand since $V(\mathbb{s} \approx 0 \text{ or } \infty) < 0$. This leads to a roughly diamond shape which starts to shrink since $V(\mathbb{s} \approx 1) > 0$. Thus, neither phase can sustain embedded isolated droplets of the other phase, no matter how large.

C. Asymmetric droplets

While the above stationary droplet behavior is far richer than in continuum formulations, these spatially discrete models exhibit even more diverse phenomenology as there exist families of "asymmetric" droplets with only twofold or onefold symmetry, as well as fourfold symmetric stationary droplets. For example, considering infected droplets at a low $p = 0.2060$ supporting a unique symmetric stationary droplet, there are two additional stationary droplets which are elongated; i.e., they have only twofold reflection symmetry about a single axis. Evolution to these droplets is realized
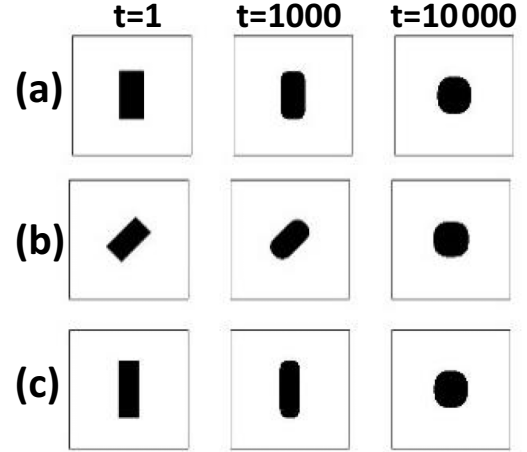

FIG. 7. Asymmetric stationary droplets for $p = 0.2060$ (middle case recovers fourfold symmetric droplet). Image size: 100×100 sites.

starting with asymmetric initial droplet shapes as shown in Fig. 7. An oblique 2×1 rectangle evolves to the unique symmetric stationary droplet with area of $A_I = 735.57$ shown in Figs. 4(b) and 5(a) for $p = 0.2060$. However, elongated vertical 2×1 and 3×1 rectangles evolve to distinct stationary droplets with sizes $A_I = 755.02$ and 787.87, respectively. Thus, behavior for $p = 0.2060$ is actually different from the traditional picture with a unique stationary droplet. In this context, it might be noted that $p = 0.2060$ is quite close to the value of $p = 0.2061$ above which multiple symmetric stationary droplets emerge.

If p is far enough below $p_-(\mathbb{s} = \infty) \approx 0.208\,09$ (e.g., for $p = 0.205$), one does recover true uniqueness; i.e., stationary infected droplets obtained from asymmetric initial shapes match those from octagonal initial shapes. On the other hand, for higher $p < p_-(\mathbb{s} = \infty)$ where there are multiple symmetric stationary droplets, we find additional asymmetric stationary infected droplets. For example, when $p = 0.207$, where there are three symmetric droplets with sizes shown in Fig. 5(b) with sizes $A_I = 1210.15$, 1380.09, and 1545.30, there exists an additional asymmetric stationary droplet with sizes $A_I = 1370.47$ obtained by starting with a 2×1 or 3×1 vertical rectangle. In the regime $p_-(\mathbb{s} = \infty) < p < p_{eq}(\mathbb{s} \to \infty)$ with infinite family of symmetric stationary droplets, there is an additional infinite set of asymmetric stationary infected droplets.

Analogous behavior is found for all-healthy droplets for high p. If p is far enough above $p_+(\mathbb{s} = 1) \approx 0.212\,73$, then there is a unique symmetric stationary droplet and no additional asymmetric stationary droplets. In fact, this is the case for $p = 0.214$ shown in Figs. 4(d)–4(f) (see the Supplemental Material [39]), noting that this p still significantly exceeds the value of $p = 0.212\,77$ below which multiple symmetry stationary droplets exist. However, for lower p, asymmetric stationary droplets emerge in addition to the symmetric ones.

VI. DISCUSSION

A. Connections to nucleation phenomena

In the Introduction, we sketched the generic picture of nucleation phenomena associated with discontinuous phase

transitions both in systems in thermodynamic equilibrium with the environment at some specified temperature [23], and also for noisy bistable nonequilibrium systems [40]. Near the transition, the less stable (strictly, metastable) steady state is long lived as only rare fluctuations can induce sufficiently large supercritical droplets to trigger conversion to the more stable state. This conversion process involves nucleation of such droplets effectively at a constant rate and at random locations followed by droplet growth, and thus is governed by Kolmogorov-Avrami kinetics [41].

To assess nucleation phenomena, e.g., for our LDE-based QCP perturbed by mixing, one would add noise to the LDE where the noise amplitude would naturally be dependent on the local S population according to standard prescriptions of stochastic chemical kinetics [42]. For example, the noise amplitude would vanish in the "absorbing" all-healthy state (since infection cannot occur spontaneously). Consequently, the all-healthy state cannot undergo fluctuation-mediated evolution to the infected state. However, the noise amplitude would be nonzero in the metastable infected state for $p > p_{\mathrm{eq}}(\mathbb{S} \to 1)$. For $p > p_+(\mathbb{S} = 1)$, fluctuations would lead to the nucleation of supercritical all-healthy droplets with $A_{\mathrm{H}} > A_{\mathrm{H}}^{c+}$ which grow producing conversion to the all-healthy state. Notably, such conversion kinetics must differ in detail from traditional Avrami kinetics. Now, fluctuations can create stable stationary droplets, which persist until an additional fluctuation results in a sufficient size increase to force their growth. This is in contrast to behavior in continuum theories where there is a unique unstable critical droplet and droplets either grow or shrink when their size is above or below this critical value, respectively. Behavior for $p_{\mathrm{eq}}(\mathbb{S} \to 1) < p < p_+(\mathbb{S} = 1)$ is fundamentally different from Avrami kinetics. Now, fluctuations initially create one of an infinite number of stationary all-healthy droplets, but if isolated these cannot grow, no matter how large. Complete conversion to the all-healthy state requires percolative overlap of individual droplets creating diagonal interfaces which can expand.

Adding noise to the QCP perturbed by spontaneous infection, now fluctuations also occur in the mostly healthy steady state which induces conversion to the infected state for $p < p_{\mathrm{eq}}(\mathbb{S} \to \infty)$. Just as above, behavior would differ from traditional Avrami kinetics somewhat for $p < p_-(\mathbb{S} = \infty)$ and dramatically for $p_-(\mathbb{S} = \infty) < p < p_{\mathrm{eq}}(\mathbb{S} \to \infty)$.

B. Brief remarks on beyond-mean-field treatments and behavior

The QCP rules specified in Sec. II A define a stochastic lattice-gas model, the precise behavior of which can be assessed by kinetic Monte Carlo (KMC) simulation. There exist KMC studies for the basic Durrett version model [22], and also for versions perturbed by mixing [30] or by spontaneous infection [43]. There also exists a KMC study for a basic threshold version including its perturbation by spontaneous infection [28]. For the combinatorial version of the QCP, KMC analysis just exists for the basic model [29]. The key qualitative features of behavior are similar to those predicted in the mean-field treatment (with suitable interpretation), but all features including the spinodal and equistability points are shifted to substantially smaller p. Spinodal points are difficult to assess (and actually cannot be precisely defined) in the

stochastic model as a result of strong fluctuations. However, all the stochastic models with various choices of rates and without and with small perturbation exhibit a well-defined regime of generic two-phase coexistence [22,28,29,30,43]. This regime corresponds to that identified by our mean-field treatment, where it is significant to note that the regime corresponds to $p_{\mathrm{eq}}(\mathbb{S} \to \infty) < p < p_{\mathrm{eq}}(\mathbb{S} \to 1)$. The values of $p_\pm(\mathbb{S} = \infty)$ and $p_\pm(\mathbb{S} = 1)$ do not determine this regime. To understand this feature, consider the vertical interface $\mathbb{S} = \infty$ which has a perfectly straight featureless form. This is in contrast to interfaces with $\mathbb{S} \gg \infty$ which can be regarded as straight interfaces with some "defect" kink sites. The latter situation corresponds better to interfaces in the stochastic model where fluctuations generate defects.

In addition to KMC simulation, beyond-mean-field analysis of model behavior is possible from higher-order truncation approximations to the appropriate homogeneous and heterogeneous master equations [34,35]. The mean-field treatment corresponds to the lowest-order site approximation, and even the next higher order pair approximation greatly improves prediction of the spinodal and equistability point locations.

VII. CONCLUSIONS

There are multiple versions of the basic quadratic contact process (QCP) with distinct choices of rates, $k_{n \geqslant 2}$. These all suffer from the quirk that a rectangular infected droplet cannot expand into or invade an all-healthy background state, and that a semi-infinite infected state cannot invade an all-healthy state separated from it by a vertical or horizontal interface. However, various perturbations of the basic model remove the quirk. Introducing exchange of neighboring H and S at small rate h removes the model quirk while preserving the all-healthy steady state. If the model perturbation involves spontaneous infection with small rate ε (rather than mixing), then the all-healthy steady state is replaced by a mostly healthy state with a small infected population. If instead infection is induced by a single sick neighbor with small rate ε, then again the all-healthy steady state is preserved. In all cases, the stable and unstable infected steady states are perturbed relative to $\varepsilon = 0$ [31].

For these various model perturbations, apart from removing the quirk, other basic features of the basic model behavior such as bistability are preserved. In particular, this applies to all aspects of healthy droplet dynamics. To illustrate this feature, the Supplemental Material [39] provides descriptions of behavior for the Durrett model considered above but with spontaneous infection at rate $\varepsilon = 0.001$ (rather than mixing), and also of behavior for the threshold model perturbed by either mixing or spontaneous infection. It should, however, be noted that in the unperturbed or the perturbed models, the bistable region, and also the equistability points, $p_{\mathrm{eq}}(\mathbb{S})$, depend strongly on the prescription of the k_n.

Our analysis of heterogeneous behavior in spatially discrete nonequilibrium systems utilizing LDE relates to a substantial body of previous LDE-based studies, which focused on planar interface propagation in one-dimensional (1D) and 2D systems. The 1D nature of such propagation sometimes allows significant insight from analytical (versus numerical) investigation. It might be noted that additional 1D phenomena

such as the existence of stationary strips of finite width of one steady state embedded in the other could also be explored [34], although application appears limited. However, significantly, there has been essentially no LDE-based analysis of intrinsically 2D phenomena such as droplet dynamics, or more generally the propagation of curved interfaces. Our study advances this area of investigation where there is important application to nucleation type phenomena in bistable systems.

Our focus has been on the QCP type model for spatial epidemics. However, the type of phenomenology which we find for these models should also occur in a much broader class of diffusionless reaction models formulated on lattices exhibiting mean-field bistability. (Introduction of significant diffusion leads to large characteristic length scales and the disappearance of such features as propagation failure, behavior being effectively described by continuum formalisms.) Examples of such reaction models are the generic monomer-dimer model [6,32,44,45], and also realistic models for catalytic CO oxidation on crystalline oxide surfaces at high pressure [8,46–48]. Mean-field treatments based on homogeneous and heterogeneous master equations can be developed for these models as for the QCP [8].

In conclusion, analysis of our LDE-based formulation of spatially discrete bistable nonequilibrium systems has revealed a diversity of droplet dynamics and stationarity far richer than RDE-based descriptions of analogous continuum systems. This diversity leads to modified and sometimes dramatically different nucleation kinetics compared with the traditional picture.

[1] G. Nicolis and I. Prigogine, *Self-Organization in Nonequilibrium Systems* (Wiley, New York, 1977).

[2] A. S. Mikhailov, *Foundations of Synergetics I* (Springer, Berlin, 1994).

[3] D. Golomb and G. B. Ermentrout, Phys. Rev. Lett. **86**, 4179 (2001).

[4] C. M. Taylor and A. Hastings, Ecol. Lett. **8**, 895 (2005).

[5] S. Rulands, B. Klünder, and E. Frey, Phys. Rev. Lett. **110**, 038102 (2013).

[6] J. W. Evans, D.-J. Liu, and M. Tammaro, Chaos **12**, 131 (2002).

[7] K. Reuter, in *Modelling and Simulation of Heterogeneous Catalytic Reactions: From the Molecular Process to the Technical System*, edited by O. Deutschmann (Wiley-VCH, Weinberg, 2009), Chap. 3, p.71.

[8] D.-J. Liu, A. Garcia, J. Wang, D. M. Ackerman, C.-J. Wang, and J. W. Evans, Chem. Rev. **115**, 5979 (2015).

[9] C. E. Elmer and E. S. van Vleck, SIAM J. Appl. Math. **65**, 1153 (2005).

[10] N. E. Kouvaris, H. Kori, and A. S. Mikhailov, PLoS One **7**, e45029 (2012).

[11] N. E. Kouvaris, M. Sebek, A. S. Mikhailov, and I. Z. Kiss, Angew. Chem., Int. Ed. **55**, 13267 (2016).

[12] R. Durrett, SIAM Rev. **41**, 677 (1999).

[13] N. Nadkarni, A. F. Arrieta, C. Chong, D. M. Kochmann, and C. Daraio, Phys. Rev. Lett. **116**, 244501 (2016).

[14] J. W. Cahn, Acta Metall. **8**, 554 (1960).

[15] S.-N. Chow, J. Mattel-Paret, and E. S. van Vleck, Int. J. Bifurcation Chaos **06**, 1605 (1996).

[16] G. Fath, Phys. D (Amsterdam, Neth,) **116**, 176 (1998).

[17] J. W. Cahn, J. Mallet-Paret, and E. S. Van Vleck, SIAM J. Appl. Math. **59**, 455 (1998).

[18] I. Mitkov, K. Kladko, and J. E. Pearson, Phys. Rev. Lett. **81**, 5453 (1998).

[19] A. Hoffman and J. Mallet-Paret, J. Dyn. Differential Equations **22**, 79 (2010).

[20] A. L. Toom, in *Multicomponent Random Systems*, edited by R. L. Dobrushin and Y. G. Sinai (Marcel Dekker, New York, 1980), Chap. 18, p. 549.

[21] C. H. Bennett and G. Grinstein, Phys. Rev. Lett. **55**, 657 (1985).

[22] D.-J. Liu, X. Guo, and J. W. Evans, Phys. Rev. Lett. **98**, 050601 (2007).

[23] J. D. Gunton and M. Droz, *Introduction to the Theory of Metastable and Unstable States*, Lecture Notes in Physics Vol. 183 (Springer, Berlin, 1983).

[24] P. W. Anderson, Phys. Rev. **109**, 1492 (1958).

[25] F. Schloegl, Z. Phys. **253**, 147 (1972).

[26] S. Handjani, J. Theor. Probab. **10**, 737 (1997).

[27] S. Chatterjee and R. Durrett, Stochastic Processes Appl. **123**, 561 (2013).

[28] C.-J. Wang, D.-J. Liu, and J. W. Evans, J. Chem. Phys. **142**, 164105 (2015).

[29] D.-J. Liu, C.-J. Wang, and J. W. Evans, Phys. Rev. Lett. **121**, 120603 (2018).

[30] X. Guo, D.-J. Liu, and J. W. Evans, J. Chem. Phys. **130**, 074106 (2009).

[31] X. Guo, D. K. Unruh, D.-J. Liu, and J. W. Evans, Phys. A (Amsterdam, Neth.) **391**, 633 (2012).

[32] J. Marro and R. Dickman, *Non-equilibrium Phase Transitions in Lattice Models* (Cambridge University Press, Cambridge, 1999).

[33] R. Kutner, Phys. Lett. A **81**, 239 (1981).

[34] X. Guo, J. W. Evans, and D.-J. Liu, Phys. A (Amsterdam, Neth.) **387**, 177 (2008).

[35] C.-J. Wang, D.-J. Liu, and J. W. Evans, Phys. Rev. E **85**, 041109 (2012).

[36] For example, $\Re_{i,j} = (P_{i+1,j}P_{i,j+1} + P_{i+1,j}P_{i,j-1} + P_{i-1,j}P_{i,j-1} + P_{i-1,j}P_{i,j+1} + P_{i+1,j}P_{i-1,j} + P_{i,j+1}P_{i,j-1})/6$ for the threshold version of the QCP model.

[37] F. C. Frank, *Growth and Perfection of Crystals* (Wiley, New York, 1958), p. 411.

[38] F. C. Frank and M. B. Ives, J. Appl. Phys. **31**, 1996 (1960).

[39] See Supplemental Material at http://link.aps.org/supplemental/10.1103/PhysRevE.101.022803 for more detailed results for regimes of propagation failure and spinodals in various perturbed models; a summary of droplet behavior for the Durrett QCP perturbed by spontaneous infection; a summary of stationary infected droplet sizes for the perturbed Durrett QCP with $h = 0.01$; and a summary of all-healthy droplet sizes for the perturbed Durrett QCP with $h = 0.01$ as well as results for the dynamics of nonstationary all-healthy droplets.

[40] H. Malchow and L. Schimansky-Geier, *Noise and Diffusion in Bistable Non-equilibrium Systems* (Teubner Texte, Berlin, 1985).

[41] M. Avrami, J. Chem Phys. **7**, 1103 (1939).

[42] N. G. van Kampen, *Stochastic Processes in Physics and Chemistry* (North Holland, Amsterdam, 1981).

[43] D.-J. Liu, J. Stat. Phys. **135**, 77 (2009).

[44] R. M. Ziff, E. Gulari, and Y. Barshad, Phys. Rev. Lett. **56**, 2553 (1986).

[45] J. W. Evans, Langmuir **7**, 2514 (1991).

[46] J. Rogal, K. Reuter, and M. Scheffler, Phys. Rev. Lett. **98**, 046101 (2007).

[47] J. Rogal, K. Reuter, and M. Scheffler, Phys. Rev. B **77**, 155410 (2008).

[48] D.-J. Liu and J. W. Evans, J. Chem. Phys. **142**, 134703 (2015).